Laboratory Investigation (2021) 101:998–1010
https://doi.org/10.1038/s41374-021-00585-7

ARTICLE

Potential role for EZH2 in promotion of asthma through suppression of miR-34b transcription by inhibition of FOXO3

Bing Liu[1] · Han Sun[2] · Junxia Wang[3] · Haibin Liu[4] · Changjuan Zhao[5]

Received: 4 September 2020 / Revised: 3 March 2021 / Accepted: 3 March 2021 / Published online: 3 May 2021

Abstract

Highly expressed enhancer of zeste homolog 2 (EZH2) has been associated with many kinds of cancers and other diseases, while its functional role in asthma is largely unknown. In our study, we investigated the molecular mechanism of EZH2 in the development of asthma. An ovalbumin-induced mouse asthma model was established, followed by injection of short hairpin RNA (sh)-EZH2, overexpression-B-cell translocation gene 2 (oe-BTG2), microRNA (miR)-34b agomir as well as their corresponding controls. Next, primary bronchial epithelial cells were isolated and cultured, followed by treatment of oe-FOXO3, miR-34b inhibitor, sh-EZH2, oe-BTG2, and corresponding controls. The effects of EZH2 on inflammation were evaluated by determining levels of inflammatory factors interleukin (IL)-4, IL-5, IL-13, IL-17, and protein levels of transforming growth factor β, matrix metalloproteinase-9, and tissue inhibitor of metalloproteinases-1. The interactions between EZH2 and forkhead box O3 (FOXO3), between FOXO3 and miR-34b promoter, and between miR-34b and BTG2 were analyzed by conducting dual-luciferase reporter and chromatin immunoprecipitation assays. Notably, EZH2 and BTG2 were significantly overexpressed, while FOXO3 and miR-34b were obviously underexpressed in asthma. EZH2 silencing led to inhibited inflammation though upregulation of FOXO3, which could bind to the miR-34b promoter and facilitate its expression. In turn, miR-34b reduced BTG2 expression by targeting its 3'untranslated region. Our study provides evidence that EZH2 promotes asthma progression by regulating the FOXO3-miR-34b-BTG2 axis.

Introduction

Asthma is a common chronic airway disorder afflicting over 300 million people worldwide [1]. Asthma is an urgent public health problem both in developing and developed countries, compounded by frequently late diagnosis and poor treatment [2]. While asthma is often diagnosed in childhood, it can arise in all age groups [3]. Previous data have revealed that age did not correlate with the risk of getting asthma, whereas other work shows that cold, obesity, smoking, and certain other stimuli contribute to asthma progression [4, 5]. Asthma is usually accompanied with chronic airway inflammation [6], which can lead to airway remodeling. Therefore, a better understanding of the molecular mechanism in asthma is urgent for targeted asthma diagnosis and treatment.

Enhancer of zeste homolog 2 (EZH2), a histone methyltransferase serving as a catalytic subunit of polycomb repressive complex 2 (PRC2), can catalyze tr-methylation of histone H3 at Lysine 27, leading to reduced expression of its target genes, which are involved in various diseases including asthma [7, 8]. Notably, previous studies have indicated conspicuously downregulated expression of EZH2 in asthma. Forkhead box O3 (FOXO3), a well-established tumor suppressor gene, has been reported to be a target gene of EZH2 [9, 10], whereas other research showed that EZH2 could mediate the expression of FOXO3 in breast cancer through apparent modification of the promotor [11]. FOXO3 acts as a transcription factor participating in the regulation of microRNA (miRNA or miR) transcription [12]. It has been

✉ Changjuan Zhao
zhaochangjuan5569@163.com

[1] Departments of Pediatrics, Linyi People's Hospital, Linyi, P. R. China

[2] Clinical Laboratory, Linyi People's Hospital, Linyi, P. R. China

[3] The 1st Ward, Departments of Pediatrics, Huantai People's Hospital, Zibo, P. R. China

[4] The 2nd Department of Pediatrics, Linyi People's Hospital, Linyi, P. R. China

[5] Pediatric Intensive Care Unit, Linyi People's Hospital, Linyi, P. R. China

reported that overexpression of FOXO3 stimulates the expression of miR-34b, thereby suppressing inflammatory cytokine levels in airway epithelial cells in breast cancer [13]. miRNAs, which are small noncoding RNA molecules, are among the key mechanisms in regulation of gene expression, and have been implicated in the patho-mechanism of asthma [14]. To be specific, expression patterns of miRNAs play crucial roles in inflammation and pathological remodeling through activation of airway structural cells and immune cells and the promotion of cytokine generation [15]. One previous publication demonstrated that the overexpression of miR-34/449 suppressed fibrosis, fibrosis-related factors, and proinflammatory cytokines by targeting insulin-like growth factor binding protein-3 (IGFBP-3) [16]. Moreover, miR-34b overexpression has been reported to relieve high glucose-induced inflammation in human HK-2 cells [17]. Furthermore, there was a correlation between miR-34b and IGFBP-3 expression. Although numerous studies have reported that miRNAs are critically involved in the regulation of asthma progression, the dynamics of miR-34b expression during asthma progression remains to be established exclusive. Since identifying the upstream of miRNA may shed light on molecular treatment targets for asthma, we performed gain and loss of function assays to demonstrate a novel role of EZH2 in asthma progression.

Materials and methods

Bioinformatics analysis

Downstream targets of EZH2 were predicted using the RNAInter (http://www.rna-society.org/rnainter/), StarBase (http://starbase.sysu.edu.cn/), and POSTAR databases (http://lulab.life.tsinghua.edu.cn/postar/). The resultant candidate genes were then overlapped by Jvenn (http://jvenn.toulouse.inra.fr/app/example.html). String (https://string-db.org/) was used to analyze gene interaction network with minimum the required interaction score set as 0.4, with visualized by Cytoscape 3.5.1. Genecards (https://www.genecards.org/) to analyze the asthma-related genes, followed by intersection by jvenn. Downstream targets of miR-34b were predicted by the RNAInter, StarBase, and RNA22 databases (https://cm.jefferson.edu/rna22/).

Study subjects

Specific pathogen-free female BALB/c mice ($n = 56$, 18–22 g, 6–8 weeks old) were obtained from Jiling University Laboratory Animal Center. Mice were maintained under controlled standard conditions (12-h-light/dark cycle, humidity 55 ± 5%, temperature 22 ± 2 °C) with free access to food and water.

Establishment of ovalbumin (OVA)-induced mouse asthma models and treatment

The mice were divided into seven groups (eight mice per group): normal control, OVA-induce asthma, OVA + short hairpin RNA-negative control (sh-NC) + overexpression (oe)-NC, OVA + oe-NC + sh-EZH2, OVA + sh-EZH2 + oe-B-cell translocation gene 2 (BTG2), OVA + NC agomir, and OVA + miR-34b agomir. Mice were injected with viruses carrying oe-NC, oe-BTG2, sh-NC, sh-EZH2, NC agomir, and miR-34b agomir via tail vein at a dose of 5×10^8 plaque forming units/mouse. To prepare the experimental allergic asthma model, mice were immunized via intraperitoneal injections of OVA (25 μg/mouse) (A-5253, Sigma-Aldrich Chemical Company, St Louis, MO, USA) with aluminum hydroxide (2 mg/mouse) (V-900163, Sigma-Aldrich Chemical Company) on the 1st and 8th days. From the 15th to the 28th day, mice were exposed to 5% (w/v) OVA solution for 30 min using a nebulizer every day, and from the 30th to the 42nd day, mice were exposed to 5% (w/v) OVA solution for 30 min every 2 days. At 24 h after the last treatment, mice were euthanized by cervical dislocation under anesthesia with sodium pentobarbital and samples were collected for subsequent analysis.

Culture of primary bronchial epithelial cells (BECs)

Mice were euthanized under aseptic conditions. Separated bronchi were placed into precooled Dulbecco's modified Eagle's medium/Ham's F-12 medium (DMEM/F12) (Thermo Fisher Scientific, Inc., Waltham, MA, USA) containing streptomycin and then moved to phosphate-buffered saline (PBS) to remove the connective tissues and blood vessels. After that, the remaining bronchi tissues were digested in the medium prepared by the mixture of DMEM/F12 and Pronase at a 1:1 volume ratio for 24 h at 4 °C. After digestion, DMEM/F12 was added to the sample and mixed gently by shaking up and down and then centrifuged. Next, DMEM/F12 medium containing penicillin and streptomycin and 10% fetal bovine serum (10100147, Gibco BRL, Grand Island, NY, USA) was used to resuspend the pellet and the cells were seeded into Petri dishes. After 2 h, undetached cells were collected and seeded into collagen-coated Petri dishes and incubated at 37 °C in a humidified incubator containing 95% air and 5% CO_2. After 24 h, fresh DMEM/F12 containing growth factor was used to replace the old medium and incubation o the BECs resumed at 37 °C in a humidified incubator containing 95% air and 5% CO_2. BECs were then treated oe-NC + inhibitor NC, oe-FOXO3 + inhibitor NC, oe-FOXO3 + miR-34b inhibitor, sh-NC + oe-NC, oe-NC + sh-EZH2, and sh-EZH2 + oe-BTG2, individually. All the shRNA and overexpression plasmids containing cytomegalovirus immediate-early enhancer and

chicken beta-actin (CAG) promoters were purchased from GenePharma (Shanghai, China), which were tested before experiments. The cells were seeded in six-well plates at a density of 3×10^5 cells/well, and upon reaching approximately 50% confluence, were transfected according to the instructions of the Lipofectamine 2000 reagent kit (Invitrogen Inc., Carlsbad, CA, USA). Plasmids pCAG-Cre-IRES2-GFP (for overexpression) and pLVX-shRNA2-PURO (for shRNA) were purchased from YouBio Biotechnology Co., Ltd. (Changsha, Hunan, China). The sequences of sh-NC, inhibitor NC, and sh-EZH2 were "5-GGGUGAACUCACGUCAGAA-3," "5-CAGUACUUUUGUGUAGUACAA-3," and "5-GAGGUUCAGACGAGCUGAUUU-3," respectively.

Hematoxylin eosin (HE) staining

Lung tissues were collected, fixed in 4% paraformaldehyde for 24 h, dehydrated in ascending series of alcohol and then N-butanol, paraffin-embedded, and sectioned. The sections were then dewaxed by xylene, hydrated, and stained with HE solution (Beijing Solarbio Science & Technology Co., Ltd., Beijing, China). Thereafter, the sections were cleared with xylene, mounted in neutral resin, and observed under an optical microscope (XP-330, Shanghai Bingyu Optical Instrument Co., Ltd., Shanghai, China) in three randomly selected complete cross-sections of small and medium-sized bronchi from each mouse at 200× magnification. Image-Proplus 6.0 software was used to measure the total area of the wall (WAt), airway smooth muscle area (WAm), and ASMC number (N), and the results were expressed in units of area of the basement membrane by length. Lung inflammation was assessed from the abundance of infiltrating inflammatory cells surrounding the bronchial vessels and rated depending on the staining intensity (0, none; 1, mild; 2, moderate; 3, significant; 4, severe).

Masson's trichrome staining

Lung tissues were collected, embedded, and sectioned. The sections were then dewaxed, hydrated, and stained with Regaud hematoxylin for 5–10 min. Following this, the sections were counterstained with Masson Ponceau S acid fuchsin solution for 5–10 min. Glacial acetic acid–water solution was used to wash the sections, which were then treated by addition of 1% phosphomolybdic acid for 3–5 min. Afterwards, samples were directly stained by aniline blue and washed with 0.2% glacial acetic acid–water solution for a few seconds. After dehydration by gradient ethanol, the sections were cleared by xylene and then sealed with neutral resin, followed by observation under a microscope and analysis of collagen deposition area by the Image J software.

Enzyme-linked immunosorbent assay (ELISA)

Bronchoalveolar lavage fluid (BALF) was obtained via tracheostomy with infusion of ice-cold PBS (0.6 mL) into the lung three times (total volume of 1.2 mL). Levels of interleukin (IL)-4 (JLC3599), IL-5 (JLC3600), IL-13 (JLC3556), and IL-17 (JLC3574) in the supernatant were measured using ELISA kits according to the manufacturer's protocols. All kits were from Shanghai JingKang Biotechnology Co., Ltd. (Shanghai, China).

Eosinophil (EOS) ratio measurement

BALF was centrifuged at 1500 rpm for 10 min, the supernatant discarded, and the pellet resuspended for microscopic examination. The amount of EOS was observed and counted using a hemocytometer according to the manufacturer's instructions.

Reverse transcription quantitative polymerase chain reaction (RT-qPCR)

Total RNA was extracted using TRIzol reagents (Invitrogen) and reverse transcribed into complementary DNA (cDNA) using the Ncode TM miRNA First-Strand cDNA Synthesis kit (Thermo Fisher Scientific). RT-qPCR was performed using the Fast SYBR Green PCR kit (Applied Biosystems Inc., CA, USA) on an ABI PRISM 7300 instrument (Applied Biosystems, Foster City, CA, USA). Primers are listed in Table 1. The miR-34b level was calculated using the $2^{-\triangle\triangle CT}$ method normalized to U6.

Protein extraction and quantification

Protein extraction was performed using protease inhibitor-contained radioimmunoprecipitation assay buffer (Boster Biological Technology Co., Ltd., Wuhan, Hubei, China). The protein sample was separated using freshly prepared sodium dodecyl sulfate-polyacrylamide gel electrophoresis, electro-transferred onto polyvinylidene fluoride membranes, and probed with primary antibodies (Abcam Inc., Cambridge, UK). Immunoblots were visualized with goat anti-rabbit immunoglobulin G (IgG) (ab205719; 1:2000;

Table 1 Primer sequences used for RT-qPCR.

Target	Primer sequences
miR-34b	F: 5'-TCTATTTGCCATCGTCTA-3'
	R: 5'-CAGGCAGCTCATTTGGAC-3'
U6	F: 5'-GCTTCGGCAGCACATATACTAAAAT-3'
	R: 5'-CAGTGCGTGTCGTGGAGT-3'

miR-34b microRNA-34b, *F* forward, *R* reverse.

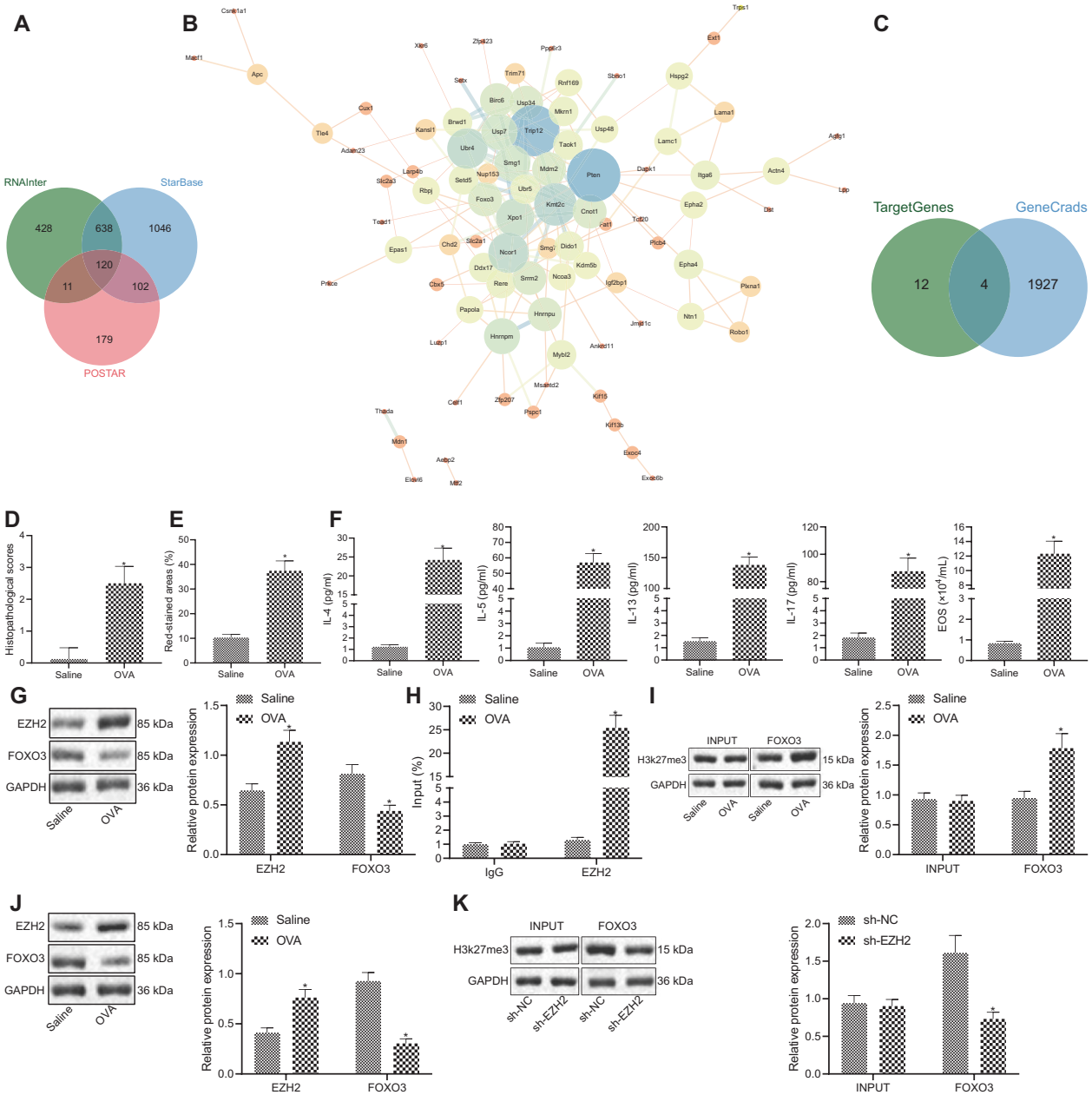

Fig. 1 EZH2 suppressed FOXO3 expression in asthma in an epigenetic manner. A Potential downstream targets of EZH2 predicted by the bioinformatics databases, RNAInter, StarBase, and POSTAR. **B** Gene interaction network analyzed by STRING; the circles in the picture represent the degree of the gene from large to small; the circle color from blue to orange indicates the degree from large to small; the line in the middle of the circle represents the interaction between genes. **C** Venn map of intersection of asthma-related genes and target genes in GeneCards database. **D** Lung tissue lesions determined by HE staining. **E** Collagen deposition analyzed by Masson's trichrome staining. **F** Inflammatory cytokines and EOS in BALF determined by ELISA. **G** Expression of EZH2 and FOXO3 determined by western blot analysis. **H** Enrichment of EZH2 in FOXO3 promoter analyzed by ChIP. **I** Enrichment of H3K27me3 in the FOXO3 promoter measure by ChIP. **J** Expression of EZH2 and FOXO3 in mouse airway epithelial cells detected by western blot analysis. **K** Enrichment of H3K27me3 in the FOXO3 promoter in mouse BECs analyzed by ChIP. $*p < 0.05$ compared to saline group or sh-NC. Statistical comparisons were performed using unpaired *t*-test when only two groups were compared or by Tukey's test-corrected one-way ANOVA with when more than two groups were compared. $N = 8$.

Abcam,) and enhanced chemiluminescence detection reagents, and then captured under the Bio-Rad image system (Bio-Rad Inc., Hercules, CA, USA). Gray value of target protein bands was quantified using the Image J software, with glyceraldehyde-3-phosphate dehydrogenase (GAPDH) used for normalization. Primary antibodies used in this assay included EZH2 (ab245738, 1:500), FOXO3 (ab70315, 1:500), BTG2 (ab197362, 1:1000), histone H3

Table 2 Determination of the value of bronchial-related indexes of normal and OVA mice.

Group	Wat/Pbm ($\mu m^2/\mu m$)	Wam/Pbm ($\mu m^2/\mu m$)	N/Pbm (N/μm)
Saline	7.41 ± 0.82	3.12 ± 0.38	0.02 ± 0.01
OVA	16.32 ± 2.11*	6.24 ± 0.71*	0.06 ± 0.03*

Pbm the length of the basement membrane of the epithelium, *Wam* the area of smooth muscle.

*$p < 0.05$ compared to Saline group. Statistical comparisons were performed using unpaired *t*-test when only two groups were compared or by Tukey's test-corrected one-way ANOVA with when more than two groups were compared.

Lys27 trimethylation (H3K27me3) (ab192985, 1:1000), transforming growth factor β (TGF-β) (ab92486, 1:500), matrix metalloproteinase-9 (MMP9) (ab38898, 1:500), tissue inhibitor of metalloproteinases-1 (TIMP-1) (ab61224, 1:1000), and GAPDH (ab18602, 1:5000).

Dual-luciferase reporter assay

The target genes of miR-34b were analyzed using the biological prediction website Starbase. The plasmids were extracted according to the instructions of Omega Plasmid Extraction Kit (D6943–01, Beijing Zhijie Fangyuan Technology, Beijing, China), after which the recombinant plasmids were constructed and designated as pmirGLO-BTG2–3'untranslated region (3'UTR)-wild type (5'-GUUAGUCGAUUAAUGUGACGGA-3') and pmirGLO-BTG2–3'UTR-mutant type (5'-GUUAGUC GAUUAAUACCGUCAA-3'). Cells from each group were seeded into six-well plates at a density of 2×10^5 cells per well and transfected using the aforementioned method after the BECs had adhered to the wall. Cell lysate was collected after transfection for 48 h. The indicated BTG2 promoter region was cloned into a pmirGLO luciferase vector (Promega, WI, USA), whereupon BTG2-pro was introduced into HEK-293T cells in the presence of the indicated combination of NC-mimic or miR-34b mimic. The luciferase activity was determined using dual-luciferase assay kit (D0010, Solarbio) on a Glomax20/20 luminometer (Promega).

Chromatin immunoprecipitation (ChIP)

Cells were treated with 1% formaldehyde for 10 min to create protein–DNA crosslink, and the crosslinked chromatin was extracted and sheared by sonication. Protein A/G beads were precleared and blocked with 1% salmon sperm DNA and 1% bovine serum albumin. Total sheared chromatin was used for immunoprecipitation with either normal rabbit IgG (ab109489, 1:300. Abcam) or EZH2 (1:100, ab191250, Abcam) and H3K27me3 (1:100, ab6002, Abcam) antibody. The immunoprecipitates were washed five times, pelleted by centrifugation, and then heated at 65 °C for 4 h to break the crosslinking, followed by RT-qPCR analysis.

Statistical analysis

All data were processed using SPSS 22.0 statistical software (IBM Corp. Armonk, NY, USA). Data are shown as mean ± standard deviation from at least three independent experiments. Unless otherwise noted, statistical comparisons were performed using unpaired *t*-test when only two groups were compared or by Tukey's test-corrected one-way analysis of variance when more than two groups were compared. A value of $p < 0.05$ represents statistical significance.

Results

EZH2 suppresses FOXO3 during asthma progression

A total of 120 candidate downstream targets of EZH2 were predicted by RNAInter, StarBase, and POSTER (Fig. 1A). Meanwhile, we analyzed the gene interaction by STRING and visualized the interaction net by Cytoscape 3.5.1, which showed phosphatase and tensin homolog deleted on chromosome 10 (PTEN), thyroid hormone receptor interacting protein 12 (TRIP12), FOXO3, and other 13 genes to be at the core of the interaction net (Fig. 1B). Furthermore, PTEN, exportin 1 (XPO1), mouse double minute 2 protein (MDM2), and FOXO3 were detected to be involved in the regulation of asthma from GeneCards (Fig. 1C). Previous research demonstrated that FOXO3 was a downstream target of EZH2 [11, 12]. To investigate the regulation of FOXO3 by EZH2 in asthma, we established an OVA-induced mouse model and then analyzed mouse behaviors. Compared to the normal group, the OVA group presented with an increase in various degree of agitation, sneezing, scratching of the ears and nose, back bowing, and forelimb lifting after being exposed to the aerosol. Furthermore, analysis using HE staining and Masson's trichrome staining revealed a significant increase of inflammatory infiltration, airway smooth muscle thickening, epithelial cell damage, and collagen hyperplasia in bronchi of the OVA group ($p < 0.05$) (Fig. 1D, E and Table 2). Meanwhile, the levels of IL-4, IL-5, IL-13, and IL-17 and EOS were also significantly elevated in the BALF from the OVA-induced group compared to saline group ($p < 0.05$) (Fig. 1F). Collectively, these data indicated the successful establishment of the OVA-induced mouse model. Based on this result, we analyzed the expression of EZH2 and FOXO3 by western blot analysis in lung tissues, which showed that, compared to normal mice, EZH2 was significantly upregulated and

FOXO3 was dramatically decreased in OVA mice ($p < 0.05$) (Fig. 1G). Meanwhile, increased enrichment of EZH2 in the FOXO3 promoter was also found in the OVA group upon analysis by ChIP assay ($p < 0.05$) (Fig. 1H). Consistent with these findings, the enrichment of H3K27me3 in the FOXO3 promoter was dramatically increased in the OVA group ($p < 0.05$) (Fig. 1I). Furthermore, FOXO3 was significantly upregulated, while EZH2 was significantly downregulated in mouse BECs ($p < 0.05$) (Fig. 1J). Furthermore, enrichment of H3K27me3 in the FOXO3 promoter was dramatically decreased upon EZH2 inhibition ($p < 0.05$) (Fig. 1K). In conclusion, our data revealed that decreased expression of FOXO3 in asthma was mediated by EZH2 in an epigenetic manner.

EZH2 silencing suppresses inflammatory cytokines, TGF-β, MMP9, and TIMP-1 expression by upregulation of FOXO3

To investigate the role of EZH2 and FOXO3 in BECs, we made a double knockdown EZH2 and FOXO3 to explore their interacting functions in BECs. Western blot analysis demonstrated that silencing of EZH2 upregulated FOXO3 expression, which could be counteracted by silencing of FOXO3 ($p < 0.05$) (Fig. 2A). EZH2 silencing led to decreased IL-4, IL-5, IL-13, and IL-17 levels measured by ELISA, and depletion of FOXO3 restored the expression of these inflammatory cytokines caused by EZH2 silencing analyzed ($p < 0.05$) (Fig. 2B). Meanwhile, the protein levels of TGF-β, TIMP-1, and MMP9 were significantly downregulated in the presence of EZH2 knockdown, which could be reversed by depletion of FOXO3 ($p < 0.05$) (Fig. 2C). Collectively, EZH2 silencing inhibited inflammatory cytokine production and MMP9 and TIMP-1 expression by upregulation of FOXO3.

FOXO3 promotes the transcription of miR-34b

Previous data revealed that FOXO3 directly binds to miR-34b promoter and facilitates its expression [18]. To confirm the regulation of miR-34b by FOXO3 in asthma, we detected the expression of miR-34b in the mouse lung tissues, which showed that miR-34b was significantly downregulated in lung tissues of OVA mice ($p < 0.05$) (Fig. 3A). Meanwhile, enrichment of FOXO3 in the miR-34b promoter was also dramatically reduced in the OVA group ($p < 0.05$) (Fig. 3B). Furthermore, we overexpressed or silenced FOXO3 in airway epithelial cells ($p < 0.05$) (Fig. 3C) and found that overexpression of FOXO3 elevated miR-34b expression, which was dramatically downregulated upon FOXO3 silencing ($p < 0.05$) (Fig. 3D). Consistent with the change of miR-34b expression levels, enrichment of FOXO3 in the miR-34b promoter was significantly increased when FOXO3 overexpressed, but this effect was abolished following FOXO3 silencing ($p < 0.05$) (Fig. 3E). Taken together, our data revealed that FOXO3 could directly bind to the miR-34b promoter and facilitated its transcription.

Overexpressed FOXO3 inhibits the expression of inflammatory cytokines, TGF-β, MMP9, and TIMP-1 by upregulation of miR-34b in BECs

To confirm the role of the FOXO3-miR-34b axis in airway epithelial cells, we overexpressed FOXO3 and silenced miR-34b (Fig. 4A). Overexpression of FOXO3 upregulated miR-34b expression, which could be reversed by inhibition of miR-34b (Fig. 4B). The inflammatory cytokines, IL-4, IL-5, IL-13, and IL-17 were dramatically decreased when FOXO3 was overexpressed, but miR-34b silencing restored the downregulation of these cytokines caused by FOXO3 overexpression ($p < 0.05$) (Fig. 4C). Meanwhile, TGF-β, MMP9, and TIMP-1 levels were dramatically downregulated by FOXO3 overexpression, but these effects could also be reversed by inhibition of miR-34b ($p < 0.05$) (Fig. 4D). In summary, overexpression of FOXO3 inhibited inflammatory cytokines, MMP9, and TIMP-1 expression by elevating miR-34b.

Ectopic expression of miR-34b inhibits inflammatory cytokines, TGF-β, MMP9, and TIMP-1 expression by directly targeting BTG2 in BECs

Five candidate downstream targets (NAV1, PEA15A, SLC41A1, CR1L, and BTG22) of miR-34b were predicted by RNAInter, StarBase, and RNA22 (Fig. 5A). Furthermore, according to the prediction of StarBase, miR-34b could directly bind to BTG2 (Fig. 5B). Consistent with this prediction, dual-luciferase assay demonstrated that miR-34b could directly bind to BTG2 3'UTR ($p < 0.05$) (Fig. 5C). Meanwhile, BTG2 was found to be significantly overexpressed in OVA mice ($p < 0.05$) (Fig. 5D).

Furthermore, upon overexpressing miR-34b ($p < 0.05$) (Fig. 5E), we found that BTG2 was strikingly downregulated ($p < 0.05$) (Fig. 5F), indicating that miR-34b directly bound to BTG2 and suppressed its expression. Next, we explored the role of the miR-34b-BTG2 axis in the functioning of airway epithelial cells. We overexpressed miR-34b and BTG2 in airway epithelial cells ($p < 0.05$) (Fig. 5G), and showed that downregulated BTG2 expression could be reversed by overexpression of miR-34b (Fig. 5H). IL-4, IL-5, IL-13, and IL-17 levels were significantly downregulated after miR-34b was overexpressed and ectopic expression of BTG2 restored the expression of theses cytokines ($p < 0.05$) (Fig. 5H). Consistent with this result, overexpression of BTG2 also reversed the

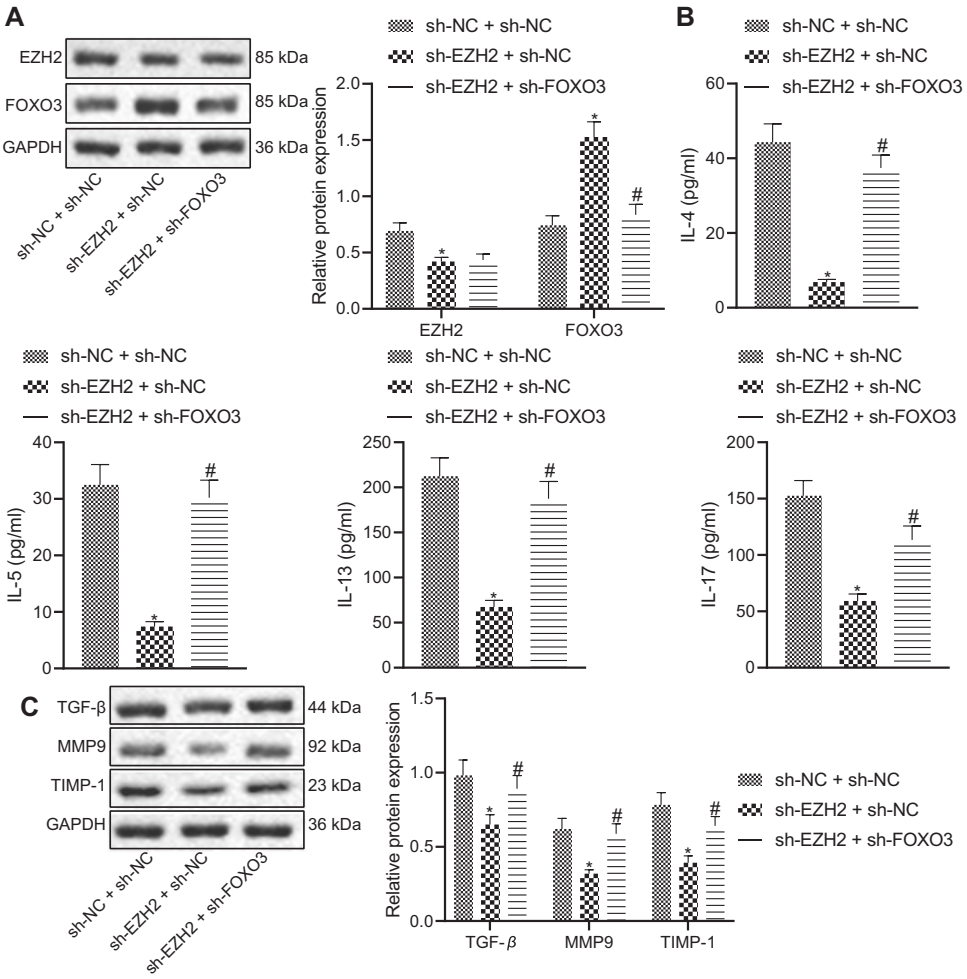

Fig. 2 Silencing of EZH2 inhibited inflammation of epithelial cells by upregulation of FOXO3. A EZH2 and FOXO3 determined by western blot analysis. **B** Inflammatory cytokines determined by ELISA. **C** TGF-β, MMP9, and TIMP-1 detected by western blot analysis. $^{*}p < 0.05$ compared to sh-NC + sh-NC. $^{\#}p < 0.05$ compared to sh-EZH2 + sh-NC. Statistical comparisons were performed by Tukey's test-corrected one-way ANOVA when more than two groups were compared.

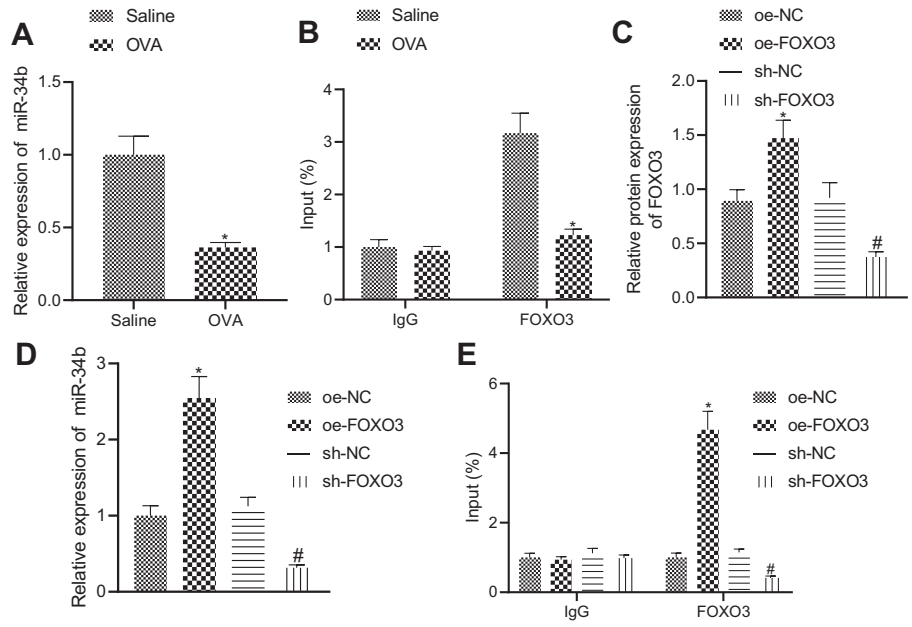

Fig. 3 FOXO3 directly binds to the miR-34b promoter and enhances its transcription. A miR-34b determined by RT-qPCR. **B** Enrichment of FOXO3 in miR-34b promoter analyzed by ChIP. **C** FOXO3 expression levels determined by western blot analysis. **D** Expression of miR-34b determined by RT-qPCR. **E** Enrichment of FOXO3 in miR-34b promoter analyzed by ChIP. $^{*}p < 0.05$ compared to Saline or oe-NC. $^{\#}p < 0.05$ compared to sh-NC. Statistical comparisons were performed using unpaired *t*-test when only two groups were compared.

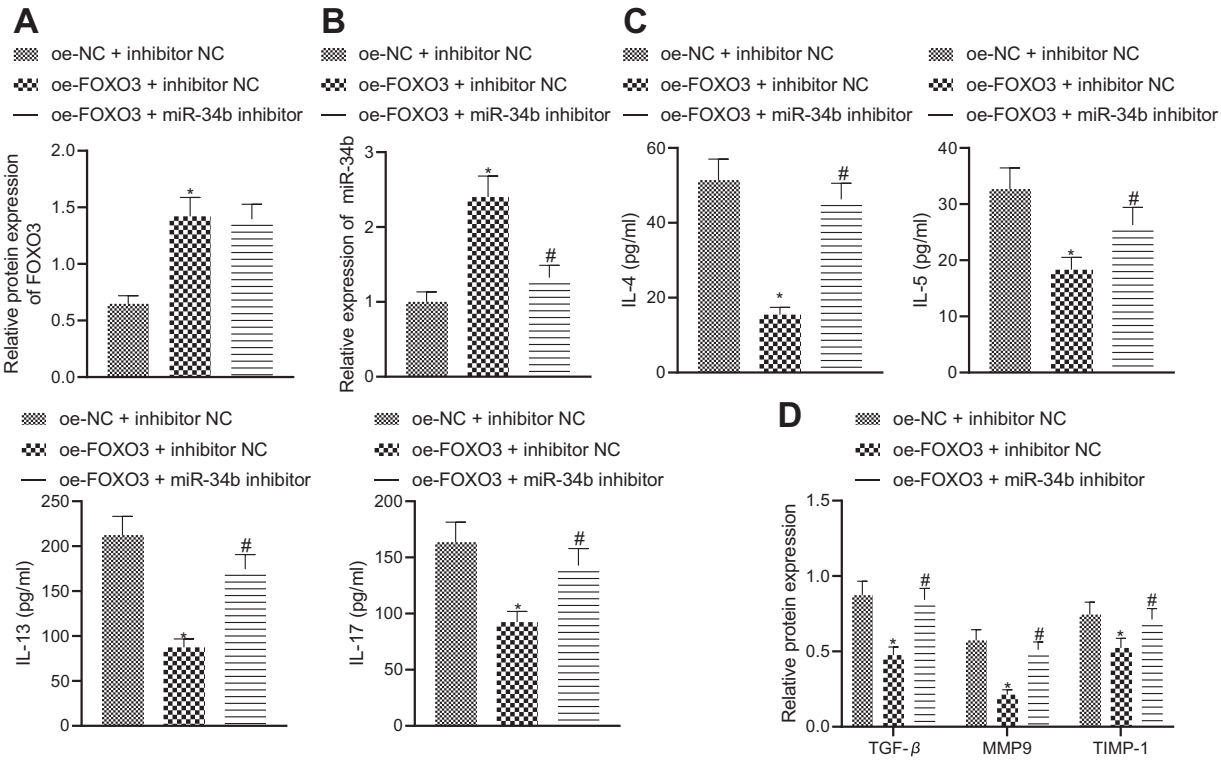

Fig. 4 Overexpression of FOXO3 suppressed inflammation and expression of TGF-β, MMP9, and TIMP-1 by facilitating miR-34b expression. A FOXO3 expression determined by western blot analysis. **B** miR-34b determined by RT-qPCR. **C** Inflammatory cytokines measured by ELISA. **D** TGF-β, MMP9, and TIMP-1 determined by western blot analysis. $^{*}p < 0.05$ compared to oe-NC + inhibitor NC. $^{\#}p < 0.05$ compared to oe-FOXO3 + inhibitor NC. Statistical comparisons were performed by Tukey's test-corrected one-way ANOVA when more than two groups were compared.

downregulation of TIMP-1, MMP9, and TGF-β caused by miR-34b overexpression ($p < 0.05$) (Fig. 5I). Taken together, ectopic expression of miR-34b suppressed inflammatory cytokines and TIMP-1 and MMP9 by downregulation of BTG2.

EZH2 silencing inhibits inflammatory cytokines, TGF-β, MMP9, and TIMP-1 expression by BTG2 through regulation of FOXO3-miR-34b axis in BECs

To verify whether EZH2 affected airway epithelial cells function by BTG2, we silenced EZH2 and overexpressed BTG2 to test their regulatory function in BECs. Western blot analysis demonstrated that silencing of EZH2 downregulated BTG2 expression, which could be reversed by overexpression of BTG2 ($p < 0.05$) (Fig. 6A). Consistent with previous data, EZH2 silencing led to downregulation of IL-4, IL-5, IL-13, and IL-17 and overexpression of BTG2 restored the expression of these cytokines (Fig. 6B). Meanwhile, re-expressed BTG2 also reversed the downregulation of MMP9, TIMP-1, and TGF-β caused by depletion of EZH2 ($p < 0.05$) (Fig. 6C). Taken together, our data revealed that EZH2 silencing downregulated inflammatory cytokines, MMP9, and TIMP-1 by FOXO3-miR-34b-BTG2 axis in BECs.

EZH2 silencing suppresses asthma progression in vivo through regulation of the FOXO3-miR-34b-BTG2 axis

Finally, we established an OVA-induced mouse model of asthma, and tested the effects of treatments with sh-EZH2, oe-BTG2, or miR-34b agomir to further explore their regulatory functions in asthma. FOXO3 and miR-34b were dramatically upregulated in EZH2 silenced lung tissues. Meanwhile, BTG2 was strikingly reduced in EZH2 silenced lung tissue. Furthermore, miR-34b overexpression led to a dramatic downregulation of BTG2 ($p < 0.05$) (Fig. 7A, B). Based on these results, we analyzed the lung tissues by HE staining, which showed that, much as with EZH2 silencing, miR-34b overexpression led to reduced inflammatory infiltration and histopathological scores. Meanwhile, BTG2 overexpression restored the reduced inflammatory infiltration and histopathological scores caused by EZH2 silencing ($p < 0.05$) (Fig. 7C). On the other hand, Masson's trichrome staining results revealed that EZH2 silencing or miR-34b

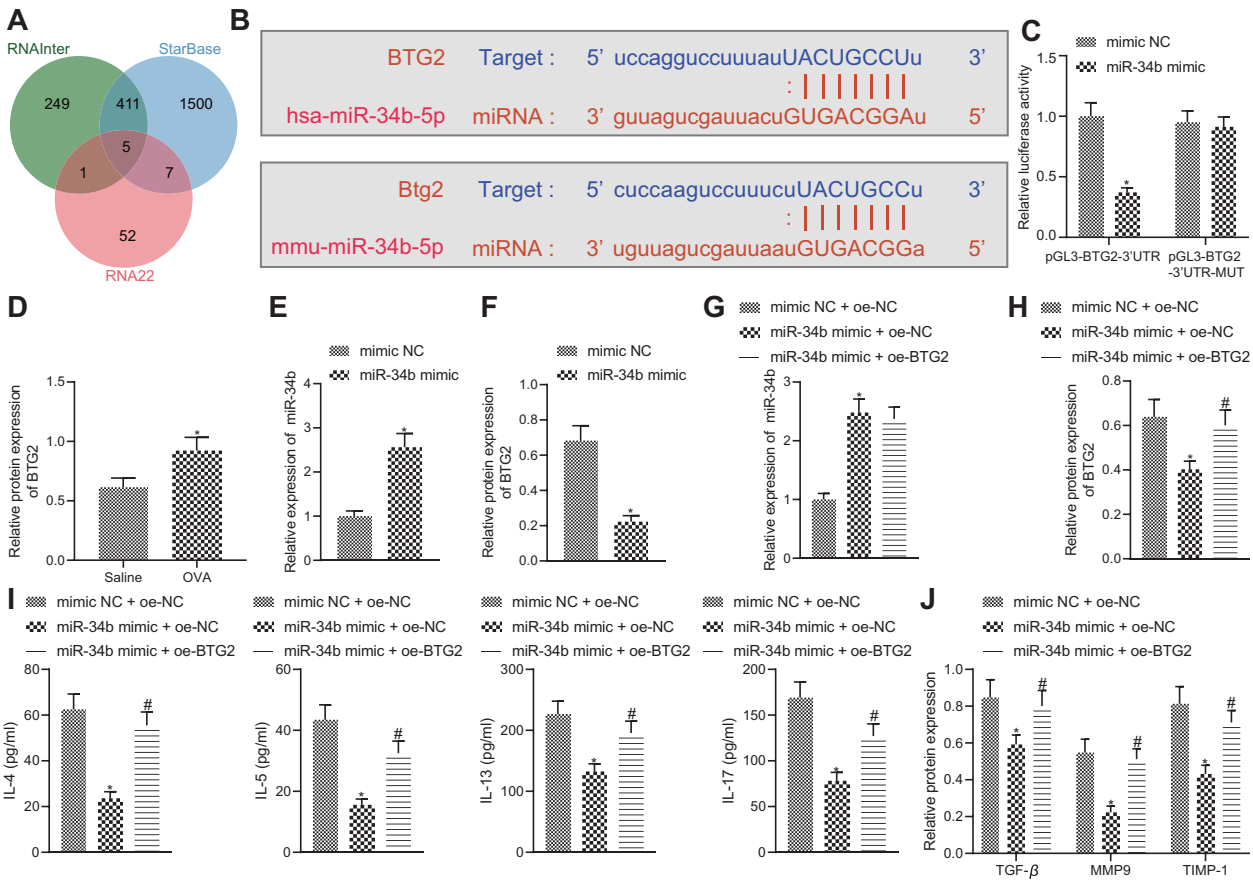

Fig. 5 miR-34b suppressed inflammation in BECs by directly targeting BTG2. A Downstream targets of miR-34b predicted by RNAInter, StarBase, and RNA22. **B** Binding sites of miR-34b in BTG2 predicted by StarBase. **C** miR-34b binding to BTG2 verified by dual-luciferase assay. **D** BTG2 expression determined by western blot analysis in normal and OVA mice. **E** miR-34b measured by RT-qPCR after treatment of miR-34b mimic. **F** BTG2 expression determined by western blot analysis after treatment with miR-34b mimic. **G** miR-34b measured by RT-qPCR. **H** BTG2 expression in each group determined by western blot analysis after treatment with miR-34b mimic or oe-BTG2. **I** Inflammatory cytokines measured by ELISA. **J** TGF-β, MMP9, and TIMP-1 determined by western blot analysis after treatment with miR-34b mimic or oe-BTG2. $^{*}p < 0.05$ compared to mimic NC + oe-NC. $^{\#}p < 0.05$ compared to miR-34b mimic + oe-NC. Statistical comparisons were performed using unpaired *t*-test when only two groups were compared or by Tukey's test-corrected one-way ANOVA with when more than two groups were compared.

overexpression reduced the surface area of mouse lung collagen deposition. Consistent with HE staining results, ectopic expression of BTG2 also reduced the collagen deposition area provoked by depletion of EZH2 ($p < 0.05$) (Fig. 7D). Furthermore, similar to effects of EZH2 silencing, miR-34b overexpression led to reduced IL-4, IL-5, IL-13, IL-17, and EOS levels in the BALF. Meanwhile, re-expression of BTG2 reversed the effects on expression of these cytokines and EOS in EZH2 silenced lung tissues ($p < 0.05$) (Fig. 7E). Consistent with the above, HE staining revealed that WAt, WAm, and the number of ASMC-stained nuclei were significantly downregulated in the lung tissue of model mice upon EZH2 silencing or miR-34b overexpression. Restoration of BTG2 in EZH2 silenced lung tissues did not result in any such effect ($p < 0.05$) (Table 3). In summary, EZH2 promoted asthma progression via regulation of the FOXO3-miR-34b-BTG2 axis in vivo.

Discussion

EZH2, a core component of PRC2 complex, regulates various biological processes such as cell cycle transition, metastasis, and chemo-resistance by remodeling chromatin methylation status through its catalytical activity [19–21]. Meanwhile, EZH2 also regulates signaling pathways by methylating non-histone proteins [22]. Previous research demonstrated that EZH2 played a role in asthma progression [8]. In this study, we established an OVA-induced mouse model and performed gain and loss of function analyses to demonstrate that elevation of EZH2 and BTG2 was essential for asthma development, thus casing light on EZH2 as a potential drug target for asthma treatment.

Asthma is a chronic inflammatory disease of the airways [23]. Inflammatory cytokines, IL-4, IL-5, IL-13, and IL-17 belong to the type 2 cytokines that are essential for regulating

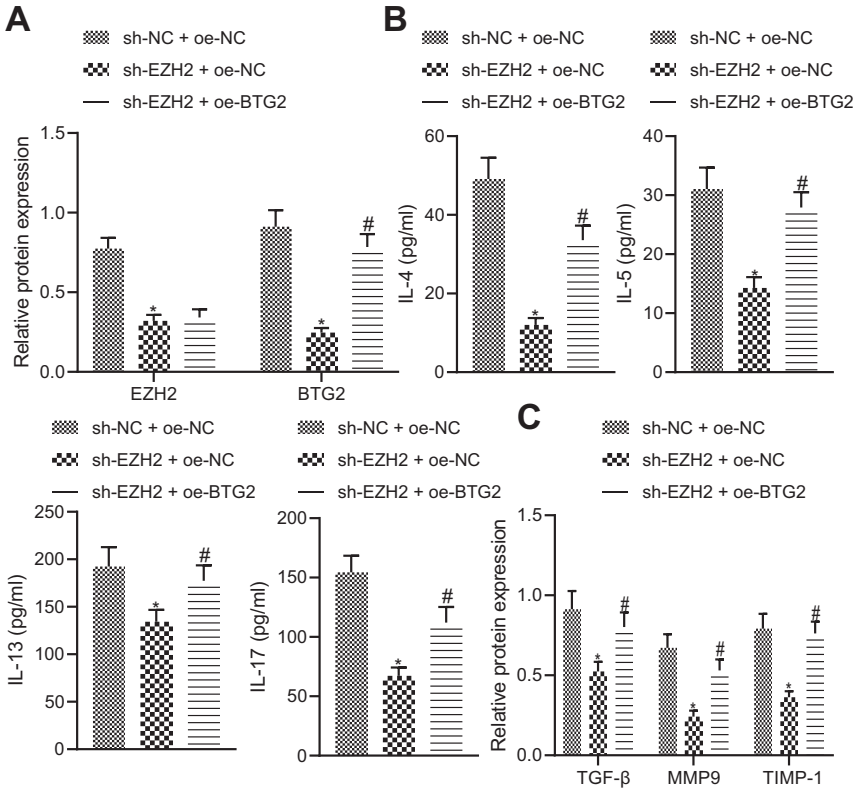

Fig. 6 EZH2 silencing inhibited inflammatory cytokines expression by FOXO3-miR-34b-BTG2 axis. **A** EZH2 and BTG2 measured by western blot analysis. **B** Inflammatory cytokines measured by ELISA. **C** TGF-β, MMP9, and TIMP-1 determined by western blot analysis. $^{*}p < 0.05$ compared to sh-NC + oe-NC. $^{\#}p < 0.05$ compared to sh-EZH2 + oe-NC. Statistical comparisons were performed by Tukey's test-corrected one-way ANOVA when more than two groups were compared.

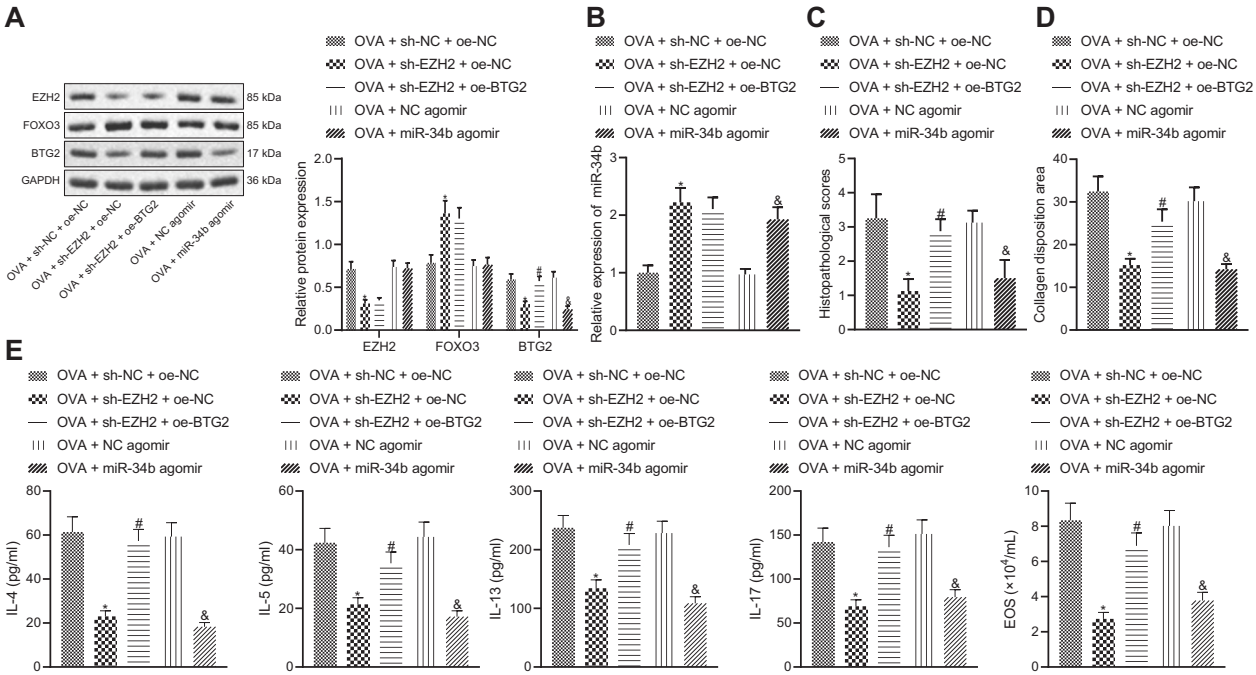

Fig. 7 Depletion of EZH2 inhibited asthma progression in vivo by FOXO3-miR-34b-BTG2 axis. **A** EZH2, FOXO3, and BTG2 expression detected by western blot analysis. **B** miR-34b measured by RT-qPCR. **C** Lung tissue lesions determined by HE staining. **D** Collagen deposition analyzed by Masson's trichrome staining. **E** Inflammatory cytokines and EOS in BALF determined by ELISA. $^{*}p < 0.05$ compared to OVA + sh-NC + oe-NC. $^{\#}p < 0.05$ compared to OVA + sh-EZH2 + oe-NC. $^{\&}p < 0.05$ compared to OVA + NC agomir. Statistical comparisons were performed by Tukey's test-corrected one-way ANOVA when more than two groups were compared.

Table 3 Determination of the value of bronchial-related indexes of mice after different treatment.

Group	Wat/Pbm (μm²/μm)	Wam/Pbm (μm²/μm)	N/Pbm (N/μm)
OVA + sh-NC + oe-NC	17.29 ± 2.04	7.89 ± 0.94	0.08 ± 0.03
OVA + sh-EZH2 + oe-NC	9.21 ± 1.13*	2.63 ± 0.31*	0.03 ± 0.01*
OVA + sh-EZH2 + oe-BTG2	16.72 ± 1.88#	6.92 ± 0.73#	0.07 ± 0.02#
OVA + NC agomir	18.19 ± 2.33	7.47 ± 0.82	0.09 ± 0.03
OVA + miR-34b agomir	10.32 ± 1.47&	4.01 ± 0.48&	0.02 ± 0.01&

*$p < 0.05$ compared to OVA + sh-NC + oe-NC group. #$p < 0.05$ compared to OVA + sh-EZH2 + oe-NC group. &$p < 0.05$ compared to OVA + NC agomir group. Statistical comparisons were performed using unpaired *t*-test when only two groups were compared or by Tukey's test-corrected one-way ANOVA with when more than two groups were compared.

allergic responses such as production of IgE, inflammatory reaction, and airway hyperresponsiveness in asthma patients [24]. As is well known, these inflammatory cytokines are produced by T helper (Th) cells. Ever mounting evidence has revealed that epigenetic modification plays a vital role in regulation of the production of type 2 cytokines by Th cells [25]. Consistent with this, a recent study revealed that EZH2 is a central regulator of invariant natural killer T (iNKT) pathogenicity and suppresses the ability of iNKT cells to induce asthma-like pathology [8]. Likewise in the present study, higher levels of EZH2 were found in the lung tissues of OVA-induced asthma mice in our study. Furthermore, we identified FOXO3 as a downstream target of EZH2. Consistent with present results, earlier research demonstrated the involvement of FOXO3 in inflammatory process [26]. Furthermore, FOXO3 is involved in the regulation of T-cell apoptosis and suppression of T-cell activation [27]. Moreover, the ability of FOXO3 to reduce production of proinflammatory cytokines has also been reported [28]. Our data in vitro showed that FOXO3 silencing could restore the reduced production of inflammatory cytokines caused by EZH2 depletion, which indicate that EZH2 promotes asthma progression by FOXO3.

miRNAs are involved in diverse biological process [29], and several studies have shown their participation in the regulation of asthma [30, 31]. Due to established role of FOXO3 in regulation of miRNAs transcription, we identity that an miRNA as an effective modulator in the EZH2-FOXO3-mediated progression of asthmamiR-34b, a potential downstream target of FOXO3, was found to be downregulated in asthma lung tissues in which FOXO3 had low expression. Furthermore, we confirmed that FOXO3 directly bound to miR-34b promoter and facilitated its transcription. Previous evidence that focused on genome wide profiling of bronchial epithelial brushings pointed revealed that miR-34/449 family members, including miR-34b-5p, were downregulated in asthma [32]. Furthermore, significantly lower miR-34b/c expression was also observed in the OVA-challenged group of mice [33]. Based on this background, we conducted gain and loss of function assays, which demonstrated that miR-34b played an essential role in EZH2-mediated asthma in vivo and in vitro. Recently, BTG2 was reported to activate nuclear factor-kappaB (NF-κB) in response to reactive oxygen species, whereupon NF-κB played a role in inflammation process [34, 35]. Our study revealed that BTG2 was directly targeted by miR-34b. Furthermore, overexpressed miR-34b could inhibit inflammation and the expression of TIMP-1, MMP9, and TGF-β through downregulation of BTG2. Previous work showed that TIMP-1, MMP9, and TGF-β were all involved in the progression of asthma [36, 37]. Also as reported previously, BTG2 was highly expressed in diesel exhaust particle-induced asthma [38]. By detection of these factors in vitro and in vivo, we now have demonstrated the role of BTG2 as the key factor in the EZH2-FOXO3-miR-34b axis to promote asthma progression.

In conclusion, our study uncovered a novel role of EZH2 in the regulation of asthma development. We demonstrated the presence of a complete signaling pathway, which was essential for asthma formation. EZH2, as an epigenetic factor, promoted FOXO3 promoter levels of H3K27me3 and thereby suppressed FOXO3 expression. Downregulated FOXO3 led to low expression of miR-34b, such that BTG2, a direct downstream target of miR-34b, was upregulated in asthma and promoted asthma progression. Further investigation should focus on whether available EZH2 inhibitors are effective in the treatment of asthma.

Data availability

The datasets generated and analyzed during the current study are available from the corresponding author on reasonable request.

Acknowledgements We acknowledge and appreciate our colleagues for their valuable suggestions and technical assistance for this study.

Funding None.

Author contributions HS designed the study. HL and CZ collated the data, carried out data analyses, and produced the initial draft of the manuscript. JW and BL contributed to drafting the manuscript. All authors have read and approved the final submitted manuscript.

Compliance with ethical standards

Conflict of interest The authors declare no competing interests.

Ethics approval and consent to participate All experimental procedures involving animals were approved by the Ethics Committee of Institutional Animal Care and Use Committee of Linyi People's Hospital. Extensive efforts were made to numbers and discomfort the suffering of the included animals.

Publisher's note Springer Nature remains neutral with regard to jurisdictional claims in published maps and institutional affiliations.

References

1. Vuolo F, Abreu SC, Michels M, Xisto DG, Blanco NG, Hallak JE, et al. Cannabidiol reduces airway inflammation and fibrosis in experimental allergic asthma. Eur J Pharmacol. 2019;843:251–9.
2. Trevor J, Antony V, Jindal SK. The effect of biomass fuel exposure on the prevalence of asthma in adults in India—review of current evidence. J Asthma. 2014;51:136–41.
3. Szefler SJ, Chipps B. Challenges in the treatment of asthma in children and adolescents. Ann Allergy Asthma Immunol. 2018;120:382–8.
4. Jamrozik E, Knuiman MW, James A, Divitini M, Musk AW. Risk factors for adult-onset asthma: a 14-year longitudinal study. Respirology. 2009;14:814–21.
5. Mims JW. Asthma: definitions and pathophysiology. Int Forum Allergy Rhinol. 2015;5(Suppl 1):S2–6.
6. Bateman ED, Hurd SS, Barnes PJ, Bousquet J, Drazen JM, FitzGerald JM, et al. Global strategy for asthma management and prevention: GINA executive summary. Eur Respir J. 2008;31:143–78.
7. Gall Troselj K, Novak Kujundzic R, Ugarkovic D. Polycomb repressive complex's evolutionary conserved function: the role of EZH2 status and cellular background. Clin Epigenetics. 2016;8:55.
8. Tumes DJ, Onodera A, Suzuki A, Shinoda K, Endo Y, Iwamura C, et al. The polycomb protein Ezh2 regulates differentiation and plasticity of CD4(+) T helper type 1 and type 2 cells. Immunity. 2013;39:819–32.
9. Gong CYS, Gomes AR, Man EP, Lee HJ, Gong G. BRCA1 positively regulates FOXO3 expression by restricting FOXO3 gene methylation and epigenetic silencing through targeting EZH2 in breast cancer. Oncogenesis. 2016;5:e214.
10. Tumes DHK, Papadopoulos M, Shinoda K, Onodera A, Kumagai J. Ezh2 controls development of natural killer T cells, which cause spontaneous asthma-like pathology. J Allergy Clin Immunol. 2019;144:549–60.
11. Gong C, Yao S, Gomes AR, Man EP, Lee HJ, Gong G, et al. BRCA1 positively regulates FOXO3 expression by restricting FOXO3 gene methylation and epigenetic silencing through targeting EZH2 in breast cancer. Oncogenesis. 2016;5:e214.
12. Tsai MJ, Tsai YC, Chang WA, Lin YS, Tsai PH, Sheu CC, et al. Deducting microRNA-mediated changes common in bronchial epithelial cells of asthma and chronic obstructive pulmonary disease—a next-generation sequencing-guided bioinformatic approach. Int J Mol Sci. 2019;20:553.
13. Liu X, Feng J, Tang L, Liao L, Xu Q, Zhu S. The regulation and function of miR-21-FOXO3a-miR-34b/c signaling in breast cancer. Int J Mol Sci. 2015;16:3148–62.
14. Specjalski K, Niedoszytko M. MicroRNAs: future biomarkers and targets of therapy in asthma? Curr Opin Pulm Med. 2020;26:285–92.
15. Maneechotesuwan K. Role of microRNA in severe asthma. Respir Investig. 2019;57:9–19.
16. Yin H, Zhang S, Sun Y, Li S, Ning Y, Dong Y, et al. MicroRNA-34/449 targets IGFBP-3 and attenuates airway remodeling by suppressing Nur77-mediated autophagy. Cell Death Dis. 2017;8:e2998.
17. Lv N, Li C, Liu X, Qi C, Wang Z. miR-34b alleviates high glucose-induced inflammation and apoptosis in human HK-2 cells via IL-6R/JAK2/STAT3 signaling pathway. Med Sci Monit. 2019;25:8142–51.
18. Liu H, Yin J, Wang H, Jiang G, Deng M, Zhang G, et al. FOXO3a modulates WNT/beta-catenin signaling and suppresses epithelial-to-mesenchymal transition in prostate cancer cells. Cell Signal. 2015;27:510–8.
19. Gardner EC, Lok BH, Schneeberger VE, Desmeules P, Miles LA, Arnold PK. et al. Chemosensitive relapse in small cell lung cancer proceeds through an EZH2-SLFN11 axis. Cancer Cell. 2017;31:286–99.
20. Huang K, Sun R, Chen J, Yang Q, Wang Y, Zhang Y, et al. A novel EZH2 inhibitor induces synthetic lethality and apoptosis in PBRM1-deficient cancer cells. Cell Cycle. 2020;19:758–71.
21. Zingg DDJ, Schaefer SM, Tuncer E, Frommel SC, Cheng P. The epigenetic modifier EZH2 controls melanoma growth and metastasis through silencing of distinct tumour suppressors. Nat Commun. 2015;6:6051.
22. Lee ST, Li Z, Wu Z, Aau M, Guan P, Karuturi RK, et al. Context-specific regulation of NF-kappaB target gene expression by EZH2 in breast cancers. Mol Cell. 2011;43:798–810.
23. Lebold KM, Jacoby DB, Drake MG. Inflammatory mechanisms linking maternal and childhood asthma. J Leukoc Biol. 2020;108:113–21.
24. Agache I, Rocha C, Beltran J, Song Y, Posso M, Sola I, et al. Efficacy and safety of treatment with biologicals (benralizumab, dupilumab and omalizumab) for severe allergic asthma: a systematic review for the EAACI Guidelines—recommendations on the use of biologicals in severe asthma. Allergy. 2020;75:1043–57.
25. Tumes DJ, Papadopoulos M, Endo Y, Onodera A, Hirahara K, Nakayama T. Epigenetic regulation of T-helper cell differentiation, memory, and plasticity in allergic asthma. Immunol Rev. 2017;278:8–19.
26. Bouzeyen RHM, Barbouche MR, Singh R, Essafi M. FOXO3 transcription factor regulates IL-10 expression in mycobacteria-infected macrophages, tuning their polarization and the subsequent adaptive immune response. Front Immunol. 2019;10:2922.
27. Dejean AS, Beisner DR, Ch'en IL, Kerdiles YM, Babour A, Arden KC, et al. Transcription factor Foxo3 controls the magnitude of T cell immune responses by modulating the function of dendritic cells. Nat Immunol. 2009;10:504–13.
28. You H, Pellegrini M, Tsuchihara K, Yamamoto K, Hacker G, Erlacher M, et al. FOXO3a-dependent regulation of Puma in response to cytokine/growth factor withdrawal. J Exp Med. 2006;203:1657–63.
29. Rubens D, Sterns RH, Segal AJ. Postpartum renal vein thrombosis. Urol Radiol. 1985;7:80–84.
30. Wang L, Xu J, Liu H, Li J, Hao H. PM2.5 inhibits SOD1 expression by up-regulating microRNA-206 and promotes ROS accumulation and disease progression in asthmatic mice. Int Immunopharmacol. 2019;76:105871.
31. Zhao M, Juanjuan L, Weijia F, Jing X, Qiuhua H, Hua Z, et al. Expression levels of microRNA-125b in serum exosomes of

patients with asthma of different severity and its diagnostic significance. Curr Drug Metab. 2019;20:781–4.
32. Solberg OD, Ostrin EJ, Love MI, Peng JC, Bhakta NR, Hou L. et al. Airway epithelial miRNA expression is altered in asthma. Am J Respir Crit Care Med. 2012;186:965–74.
33. Ho CY, Lu CC, Weng CJ, Yen GC. Protective effects of diallyl sulfide on ovalbumin-induced pulmonary inflammation of allergic asthma mice by microRNA-144, -34a, and -34b/c-modulated Nrf2 activation. J Agric Food Chem. 2016;64:151–60.
34. Imran M, Lim IK. Regulation of Btg2(/TIS21/PC3) expression via reactive oxygen species-protein kinase C-NuFkappaBeta pathway under stress conditions. Cell Signal. 2013;25:2400–12.
35. Irving JA, Enshaei A, Parker CA, Sutton R, Kuiper RP, Erhorn A, et al. Integration of genetic and clinical risk factors improves prognostication in relapsed childhood B-cell precursor acute lymphoblastic leukemia. Blood. 2016;128:911–22.
36. Kobayashi T, Kim H, Liu X, Sugiura H, Kohyama T, Fang Q, et al. Matrix metalloproteinase-9 activates TGF-beta and stimulates fibroblast contraction of collagen gels. Am J Physiol Lung Cell Mol Physiol. 2014;306:L1006–1015.
37. Park CS, Kim TB, Moon KA, Bae YJ, Lee HR, Jang MK. et al. Chlamydophila pneumoniae enhances secretion of VEGF, TGF-beta and TIMP-1 from human bronchial epithelial cells under Th2 dominant microenvironment. Allergy Asthma Immunol Res. 2010;2:41–47.
38. Verheyen GR, Nuijten JM, Van Hummelen P, Schoeters GR. Microarray analysis of the effect of diesel exhaust particles on in vitro cultured macrophages. Toxicol In Vitro. 2004;18:377–91.